Communicating Is Crowdsourcing: Wi-Fi Indoor Localization with CSI-based Speed Estimation

Member CCF, ACM, IEEE, Ji-Zhong Zhao(赵季中)[1], Zhi-Ping Jiang(蒋志平)[1], Member ACM, Senior Member IEEE, Xiang-Yang Li(李向阳)[2,3], Member IEEE, Shao-Jie Tang(唐少杰)[4], Member CCF, ACM, IEEE, Jin-Song Han(韩劲松)[1], Member CCF, ACM, IEEE, Wei Xi(惠维)[1], Kun Zhao(赵鲲)[1], and Zhi Wang(王志)[1]

[1]*School of Electronic and Information Engineering, Xi'an Jiaotong University, Xi'an, P.R.C*
[2]*Department of Computer Science and Technology and TNLIST, Tsinghua University*
[3]*Department of Computer Science, Illinois Institute of Technology, IL, U.S*
[4]*Department of Information Science, UT Dallas, TX, U.S*

E-mail: {*zjz,hanjinsong,zhaokun2012,zhiwang*}@mail.xjtu.edu.cn; {*jiangzp.cs, weixi.cs, tangshaojie, lirui.xjtu*}@gmail.com ; *xli*@cs.iit.edu

Received submit date

摘要 Numerous indoor localization techniques have been proposed recently to meet the intensive demand for location based service (LBS). Among them, Wi-Fi fingerprint-based approaches are the most popular solutions, and the core challenge of that is to lower the cost of fingerprint site-survey. One of the trends is to collect the piecewise data from clients and establish the radio map in crowdsourcing manner, however the low participation rate blocks the practical use.

In this work, we propose a *passive crowdsourcing* CSI-based indoor localization scheme, **C^{2}IL**. Despite a crowdsourcing based approach, our scheme is totally transparent to client except the only requirement is to connect to our 802.11n APs. **C^{2}IL** is built upon an innovative method to accurately estimate the moving speed solely based on 802.11n Channel State Information (CSI). Knowing the walking speed of a client and its surrounding APs, a graph matching algorithm is employed to extract the RSS fingerprints and establish the fingerprint map. In localization phase, we design a trajectory clustering-based localization algorithm to provide precise real- time indoor localization and tracking. We developed and deployed a practical working system of **C^{2}IL** in a large office environment. Extensive evaluations indicate that the error of speed estimation is within 3%, and the localization error is within $2m$ at 80% time in very complex indoor environment.

Keywords CSI, Speed Estimation, Fingerprint Map, Graph Matching, Indoor Localization

---

This work is supported by the National Natural Science Foundation of China (NSFC) under Grant Nos. 61325013, 61190112, 61170216, and 61228202; Natural Science Foundation of U.S (NSF) under Grant Nos. CNS-0832120, CNS-1035894, ECCS-1247944, ECCS-1343306; the Fundamental Research Funds for the Central Universities of China under Project No. 2012jdgz02 (Xi'an Jiaotong University), and the Research Fund for the Doctoral Program of Higher Education under project No. 20130201120016.

1 Introduction

With the prosperity of mobile devices, especially smartphones, location based services (LBS), which use the geographic position to provide targeted services, have become pervasive to provide added value of existing services. A critical challenge of LBS is to find the accurate location of mobile devices. GPS has successfully dominated the outdoor localization. Unfortunately in indoor environment, the most facile wireless received signal strength (RSS) is neither accurate nor consistent due to the highly dynamic and complex environment. As the flourishing of smartphones and crowdsourcing computation models, numerous indoor localization techniques have been proposed to collect fractional environment features and collaboratively provide precise indoor localization.

The relatively good accuracy and simplicity of fingerprint based localization schemes has attracted massive of effort in the community. Wi-Fi fingerprint- based schemes can provide meter-level indoor localization accuracy at the expense of explicit site-survey. Its high deployment cost and low adaptiveness to environment change hinders the practical effectiveness. Recently several novel techniques, *e.g.*, [1–5], have been proposed to raise the usability and accuracy. Among these approaches, a hot research trend is to incorporate crowdsourcing model and built-in sensors in today's smartphone. LiFS [5] reduces the site-survey by using the moving distance, estimated from counting the number of steps by accelerometer, as constraints for matching between the map and trace-graph, achieving average accuracy of $5.8m$ Zee [2] achieves a mean accuracy $3m$ by estimating the moving direction and moving distance by similarly leveraging the sensors in smartphone. Centuar [3] and PAL [4] both calibrate the Wi-Fi fingerprints database using acoustic ranging and they achieve $1\sim3m$ accuracy. All these approaches significantly improved the practicability of Wi-Fi based indoor localization, however, we believe there are plenty of room for improving the localization accuracy while reducing or even eliminating the dependence of site-survey and noisy inertial sensors.

In this work, we design and develop an indoor localization system **C^{2}IL** with even lower cost and hindrance. Our scheme exploits the Channel State Information (CSI) introduced in 802.11n Spec., for better speed estimation which in turn results in a better fingerprints matching and localization. Additionally, **C^{2}IL**, as in most recent techniques, collects the WiFi RSS fingerprints during communication between the user and WiFi APs, and populates the fingerprints database by crowdsourcing. **C^{2}IL** has good performance in complex environment with rich multipath effect, while several recently developed schemes suffer from lower localization accuracy in such a complex environment.

The accurate moving speed estimation is based on the readily available CSI in IEEE 802.11n system that uses OFDM and Multi-Input & Multi-Output (MIMO) technologies. CSI measures the inherent channel propagation decay for each subcarrier of the underlying OFDM system. Since CSI focuses more on small- scale wireless fading, it has advantages on capturing the mobile channel characteristics. In our preliminary testes carried in different scenarios, we found the CSI amplitude exhibits ripples- like Rayleigh deep fadings [6] with some periodicity across all subcarriers when the transceiver devices were moving. Fig. 1 (a) and (b) show the CSI ripples in different 802.11n Modulation and Coding Scheme (MCS)* configurations. A natural question raised in our mind is "*Are these*

802.11n uses MCS value to represent different transmission variables combinations. Higher MCS value often denotes higher rate. you may refer `www.mcsindex.com` for details.

ripples correlated with distance or speed?".

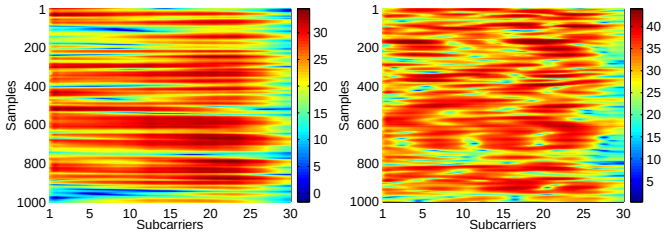

(a) Ripples in SISO (b) Ripples in MIMO

Fig. 1. (a) Ripples across nearly all subcarriers in 1×1 SISO with MCS=0. (b) The ripples in 3×3 MIMO configuration with MCS=16.

The answer is beyond an intuitive *yes*. In this work, we first exhibit a simple yet precise relationship between moving speed v and the frequency of ripples-like fadings f_r.

Based on this important discovery, we propose a simple method to precisely estimate a wireless device's moving speed (or moving distance) purely based on wireless traffic. Since in Wi-Fi environment both AP and clients can measure the CSI and RSS, the client's moving speed and RSS can be measured remotely at AP-end *passively* and *non-intrusively*. In such case, all connected devices become the participants of the crowdsourcing system without any effort.

Based on the precise speed and moving distance estimation, our localization scheme **C^{2}IL** applies the graph matching (GM) for several core tasks: Wi-Fi fingerprints extraction, automatic mapping between fingerprints and floor plan, and users localization/tracking. It has been widely known that the RSS value is affected by many factors, *e.g.*, the RSS values collected at the same location using same devices with same WiFi APs could fluctuate to a few db depending on how users hold and block the signal [1]. Such fluctuation will significantly impact the fingerprint matching quality and thus impact the localization/tracking accuracy. We first identify and successfully address the directional shadowing problem for conventional threshold-based fingerprints extraction, and we propose a trajectory matching-based solution to eliminate the shadowing problem. For fingerprints mapping task, **C^{2}IL** supports unsupervised floor plan mapping for large scale complex indoor environment. For localization/tracking task, a combination of trajectories matching and particle filter is proposed to achieve precise indoor localization/tracking. In summary, the contributions of **C^{2}IL** are as follows.

• Compared with the previous approaches with good accuracy, our scheme **C^{2}IL** does not require the localization devices to be smartphones with various inertial sensors (which are required in [2, 5]). As it only requires 802.11n connection, **C^{2}IL** has the lowest barrier on client, thus, we expect it to have better contribution from users, which is of vital importance for practical and continuously-functioning crowdsourcing system.

• **C^{2}IL** is a practical localization system that really benefits from the multipath effect, instead of suffering from this notoriously challenging effect. Theoretical analysis showed that it is exactly the multipath effect that enables the accurate distance estimation by CSI. Our extensive experimental evaluation indicated that in typical indoor scenarios, the distance estimation error is often within 3% regardless of moving speeds, which is much more accurate than Dead-Reckoning or pedometer based approaches.

• The adoption of graph matching and other techniques in our core design guarantees the accuracy and scalability of RSS radio map and localization in very large and complex environment. We design and develop a prototype of **C^{2}IL** in a large office environment of about $2000m^2$ with complex structure. In our tests, the localization error without any historical data is within $5m$; while in tracking mode, the tracking error could be within $1m$.

The rest of the paper is organized as follows. We review related techniques in Section 2, present **C^{2}IL** system overview in Section 3 and our innovative distance estimation in Section 4. Fingerprint extraction and the complete crowdsourcing based localization scheme are introduced in Section 5 and Section 6 respectively. We present the fine-grained indoor tracking solution in Section 7, and report our extensive performance evaluation of **C^{2}IL** in Section 8. We conclude the paper in Section 9.

2 Related Work

2.1 Indoor Localization Schemes

The great success of GPS [7] doesn't lead to a finish line for the localization problem. In battery constraint wireless ad-hoc network, great efforts [8, 9] have been made to bring better accuracy, and in indoor environment, the signal shadowing and multipath effect also block the GPS or similar ideas.

fall into two categories: Fingerprint-based and Modeling-based. Fingerprints are utilized in many literatures to assist positioning, and the most widely used one is WiFi signal. In indoor environment, fingerprint based methods (*e.g.*, Radar [10], Horus [11]„ SurroundSense [12], PinLoc [13],) first collect fingerprint of WiFi signal (or cellular, or FM, or other sensors such as light) in advance at known locations inside a building, and then identify the user's location by matching the fingerprint of this user with the fingerprint stored in database. Dead-Reckoning is another stream of techniques (*e.g.*, [2, 14, 15]) proposed in the literature for localization.

The mostly used fingerprint is the RSS value. LiFS [5] proposed a crowdsourcing based indoor localization, which exploits the possibility of automatically establishing the mapping between fingerprint set F and position set P In our previous work [16], graph matching algorithm is used to achieve the automatic mapping in complex environment. Acoustic ranging (AR) assisted Wi-Fi positioning was recently developed to provide distance estimation between two users (*e.g.*, [3, 4]). These schemes leverage the accurate AR and are able to provide high localization accuracy using the mapping of fingerprints with some additional distance constraint.

CSI has potential for accurate indoor localization since the CSI tool [17] has been released to public on off-the-shelf hardware. CSI is not a simple extension of RSS on physical subcarriers but it reveals totally different information on frequency selective fading process [18]. SpinLoc [1] proposed a rotation based indoor localization system that leveraged the human bodies' strong fading to Line-of-Sight (LoS) components. PinLoc [13] proposed a CSI fingerprint-based localization system which can achieve meter-level precise indoor point localization. Based on the strong position distinction property of CSI, CSITE [19] proposed an Wi-Fi Management Frame Authentication framework. Besides the above device-based localization, FrogEye [20] proposed an CSI-based device-free crowd density estimation system. Twins [21] proposed an critical state based device-free tracking system. Compared with these schemes, our scheme provide an accurate moving speed estimation of a single user in a complex indoor environment.

Recently, the popularity of Software Defined Radio (SDR) system brings more powerful approaches. ArrayTrack [22] use an antenna array driven by SDR to provide accurate Angle-Of-Arrival (AoA) based indoor localization. On the other hand, Wi-See [23] and PinIt [24] simulate the antenna array by a moving antenna. The latest work WiTrack [25] implements Frequency-modulated continuous-wave (FMCW) radar technology on SDR platform, and it achieves 3D device-free human tracking. Although SDR plat-

form exhibits strong potential, the deployment cost and computation requirement are still too high for wide range deployment.

2.2 Estimate Moving Speed by Wireless Signal

There is a long history of estimating moving velocity of a mobile station according to wireless signal [26, 27]. Most of them focused on fast moving stations, *i.e.*, a mobile station in cars or trains. However, the algorithm for estimating the maximum Doppler frequency f_d, on which most of these methods based, is not suitable for estimating human walking speed. The maximum Doppler frequency in 2.4G or 5G Wi-Fi environment could be almost totally ignored, *i.e.*, for a moving station with a velocity $1.5m/s$, f_d is merely 12Hz/25Hz compared to the carrier frequency 2.4Ghz or 5.2Ghz.

To the best of our knowledge, [28] is the only previous work that implemented an indoor speed estimation system, which is based on DVB-T signal working at 746Mhz. This work used the relationship $v = \xi\frac{\lambda}{T_c}$ to estimate velocity, where $\xi = 0.423$ a pre-defined constant, λ the wavelength, and T_c is the channel coherent time. However, for Wi-Fi signal with small covering range, which causes non-uniformly Rayleigh fading, a constant ξ is not appropriated, and it is very difficult and challenging to precisely estimate the ξ in a dynamic indoor environment.

2.3 Graph Matching via Relaxation

Graph matching (GM) is a widely used technique to find the best correspondence between two graphs, documents, or images. In **C^{2}IL**, we use GM to extract RSS fingerprints and automatically establish the mapping between RSS fingerprints and floor plan.

GM is essentially an integer quadratic programming (IQP) problem,and it is NP-hard [29]. Given two graphs $G^P = (\mathcal{V}^P, \varepsilon^P)$ and $G^Q = (\mathcal{V}^Q, \varepsilon^Q)$, the goal of GM is to find the best correspondence between two graphs. Let $C^{P\times Q}$ represent the possible matching candidates set, the affinities between all candidates are recorded in an adjacency matrix $\mathcal{M}^{C^{P\times Q}}$ based on applications. Let $\mathcal{X} \in \{0,1\}^{n^{\mathcal{M}}C^{P\times Q}}$ be a column-wise binary vector which indicates the selected correspondences, the graph matching problem can be expressed as finding the best indicator vector $\mathcal{X}^*$ that maximizes a score function $S(\mathcal{X}) = \mathcal{X}^T\mathcal{M}^{C^{P\times Q}}\mathcal{X}$, *i.e.*, $\mathcal{X}^* = \operatorname{argmax} S(\mathcal{X})$.

Various relaxation based methods have been proposed. Most of them relax the integer constraint of $\mathcal{X}$. After obtaining the optimal $\mathcal{X}^*$ in real number domain with different insights of $\mathcal{M}$, the discretization of $\mathcal{X}^*$ will make the best approximated solution to the underlined IQP problem. In **C^{2}IL**, two major graph matching algorithms, spectral matching (SM) [30] and Reweighted Random Walks Matching (RRWM) algorithms [29] are used in different stages. SM is used in extracting RSS fingerprints graph; while RRWM is used in mapping between RSS fingerprints and floor plan.

3 Architecture Overview

Since CSI and RSS can be estimated by both APs and clients, **C^{2}IL** can be deployed in either AP-end or client-end. Whenever it is deployed at either end, the core of the system remains same. In the rest of the paper, for simplicity of presentation, we assume that WiFi APs will collect the signal and conduct the needed computation. The positions of WiFi APs are not required to be known in either case.

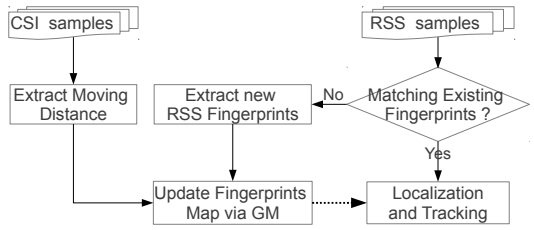

Fig. 2. **C^{2}IL** System Architecture.

Fig. 2 demonstrates our system architecture. When a user enters the building, we assume that the device held by the user will build wireless connections with the APs inside the building. The IEEE 802.11n WiFi APs will record the RSS values and the CSI values of the received signal from the client device and send the data to a localization server. Based on the sequence of the CSI values taken during a time-window, the server will then quickly estimate the moving distance of the client in this time-window. The RSS values will be used to build a matching with the fingerprint RSS values stored in the fingerprint database, which itself is populated using crowdsourcing techniques. The estimated moving distance, together with the estimated geodesic distance of different fingerprint locations in the map, will be used to further improve the quality of the matching, and thus, the accuracy of the localization. In the rest we discuss in detail each of the components in **C^{2}IL**.

4 Estimating Moving Speed by CSI

In this section, we mainly focus on the techniques of estimating moving speed and thus moving distance by CSI. Theoretical basis is presented first, and then we present our algorithm implementation.

4.1 The Electromagnetic Standing Wave Field

Wireless radio propagation in compact environment could be modelled as a superposition of large-scale path-loss, middle-scale shadowing, and small-scale multipath fading [6]. For the multipath fading, it is usually fitted to a statistical model called Rayleigh or Rician (Rayleigh fading plus strong LoS components) distribution. The ripples-like deep fading shown in Fig.1 (b) and (c) are typical Rayleigh fading pattern.

Previous speed estimation methods, are based on some statistical properties of Rayleigh distribution, *e.g.* level crossing rate (LCR) or coherent time T_c. Although it has been experimentally validated that the distance between two adjacent ripples (deep fadings) is about $\lambda/2$ (λ is the carrier wavelength) even in large-scale multipath environment (like Manhattan city) [31], no previous works explicitly exploit such $\lambda/2$ fluctuation, since such fluctuation is encapsulated and blurred in a too general model.

However, some detailed studies of radio propagation [32, 33] have indicated that, in a *complex multipath* environment the constructive or destructive interferences of the large sum of reflected and scattered waves will generate a *standing waves field*, and the environment becomes a weak *Electromagnetic Cavity Resonator* (ECR) [34] which hold standing waves in a very short time. According to basic physics of wave propagation, the distance between two adjacent *antinodes* (position with maximum amplitude), *towards any direction*, is $\lambda/2$, thereby the experimentally observed $\lambda/2$ fluctuation. Therefore, when an antenna traverses the indoor space with a speed v, a periodically ripples-like pattern with a frequency $f_o = 2\frac{v}{\lambda}$ appears. Such simple relationship inspires us that the moving speed v could be precisely estimated purely from the CSI, if we could precisely estimate the f_o.

4.2 Speed Estimation Algorithm

As previously described, the speed estimation problem now becomes a specific frequency estimation problem. We design a reasonable and effective processing flow. It includes Data Preprocessing, Noise Cancellation, Fading Enhancement, and Frequency Estimation.

Data Preprocessing: Every frame sent in 802.11n MCS rate at time t has an CSI $\boldsymbol{H}_t$. It is a complex-number vector with a length of $N_{ss} \times L_{ss}$, where N_{ss} and L_{ss} are the number of MIMO spatial streams and number of measured subcarriers across the Wi-Fi bandwidth. Every complex value $h_t^i \in \boldsymbol{H}_t$ describes the instantaneous amplitude a_t^i and phase θ_t^i of the underlying i-th subcarrier. In order to enable all 802.11n compatible devices to be ready for speed estimation, we only use the first spatial stream (first L_{ss} values in $\boldsymbol{H}_t$) to estimate speed. Moreover, the computation space is greatly reduced. Since in multipath environment the phase θ^i is uniformly distributed between $[0, 2\pi]$ [6], which provides no discriminative information. Thus we drop the phase θ_t^i and only use amplitude $\boldsymbol{A} = |\boldsymbol{H}|$ to estimate speed.

The amplitude matrix $\mathbf{A}_{ori} = \{\boldsymbol{A}_1, ..., \boldsymbol{A}_n\}^T$ is further defined, where $\boldsymbol{A}_i$ is the ith received column-wise amplitude. Since the instantaneous reception rate of frames is unstable due to the wireless traffic control, $\mathbf{A}_{ori}$ is resampled to a stable reception frequency f_w with the even interval between each slot, and let $\mathbf{A}_{re}$ denote the resampled amplitude matrix.

Noise Cancellation: Convolution based noise cancellation is applied on $\mathbf{A}_{re}$ to filter out the high frequency noise, that $\mathbf{A}_{nc} = \mathbf{A}_{re} * \boldsymbol{h}_b(r)$,

$$\boldsymbol{h}_b(r) = r \cdot \mathbf{1}^s$$

where $\mathbf{1}^s$ is a full-$\mathbf{1}$ square matrix of size s. Currently in our system $s = 6$. This step is of great importance according to the real data evaluation, since the following fading enhancement and frequency estimation is quite sensitive to noise.

Fading Enhancement: An intuitive idea of enhance the fading is first-order derivation of $\mathbf{A}_{nc}$, however, first-order derivation is quite sensitive to high frequency noise rather than low frequency ripples. Another convolution is used to emphasize the fading that $\mathbf{A}_{en} = \mathbf{A}_{nc} * \boldsymbol{h}_{df}$, where $\boldsymbol{h}_{df}$ is a Sobel-style calculator that

$$\boldsymbol{h}_{df} = \begin{bmatrix} 2 & 5 & 2 \\ 0 & 0 & 0 \\ -2 & -5 & -2 \end{bmatrix} \quad (1)$$

Fig. 3 shows the intermediate results After first 3 processing, and it is now suitable for frequency estimation.

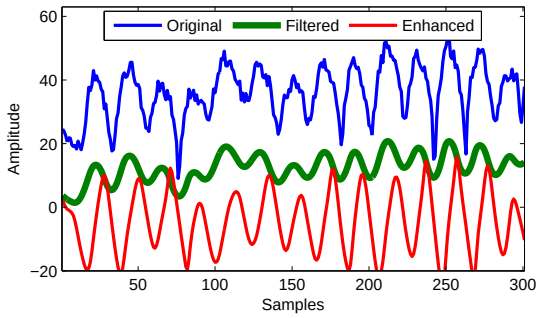

Fig. 3. The effect of each step of processing.

Frequency Estimation: Due to the MIMO configuration or other interference, deep fading(s) in all subcarriers are not guaranteed to appear simultaneously, as shown in Fig. 1, therefore the final decision of f_o are based on the estimations of each underlying subcarriers.

Extracting f_o^i for i-th subcarrier is equivalent to extracting the expected frequency $E(f_c^i)$ in the spectral graph within a frequency interval $f_{min} < f_c < f_{max}$. According to Eq. (5), f_{min} and f_{max} are set according to the speed interval of human walking that

$$f_{min} = 2 \cdot v_{min}/\lambda, \quad f_{max} = 2 \cdot v_{max}/\lambda \quad (2)$$

where the minimum speed v_{min} and the maximum speed v_{max} in our system are set to 0.8m/s and 1.6m/s.

Short-Time Fourier Transformation (STFT) with 50% overlapping window is applied to obtain the Power Spectral Density (PSD) of i-th envelope of $\mathbf{A}_{re}$. It reveals the spectral density of subcarrier i along with time. To reduce the jitter, the estimated f_o^i is set to the weighed expectation of frequencies between f_{min} and f_{max}

$$f_o^i = \frac{\sum_{f_{min}<s_j<f_{max}} s_j \cdot w_j}{\sum w_j}, \quad (3)$$

where w_j denotes the power of frequency f_j.

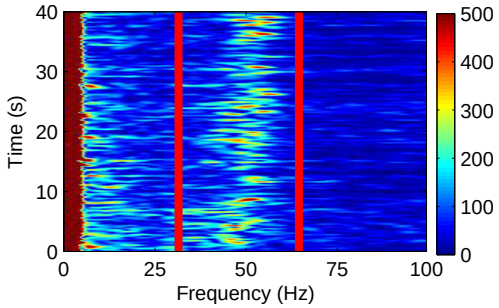

Fig. 4. STFT result for $15th$ subcarrier at 5.8Ghz (Channel 161).

Figure 4 shows the STFT result for 15-th subcarrier. We can see very strong power around 50Hz. As $50 \times \frac{\lambda}{2} = 1.29m/s$, and it is quite close to the real walking speed at about $1.3m/s$. Two red bars denote the f_{min} and f_{max}, and they are set to 32 and 64 according the v_{min} and v_{max} settings. The final estimation of f_o is set to the median of all estimated f_o^i

$$f_o = median(f_o^1, f_o^2, ...f_o^n), n = N_{ss} \quad (4)$$

Then the moving speed is estimated by

$$v = \frac{\lambda \cdot f_o}{2} \quad (5)$$

It was worth to mention that although the Doppler effect does exist, as discussed in Section 2, the Doppler frequency is small comparing to the carrier frequency. Thus in current system design, we did not consider the Doppler effect caused by human walking.

4.3 Stop Detection

Precise Start and Stop detection of human walking by wireless device is a challenging problem. Since instantaneous state shift of moving or static mainly reflect on small-scale fading, we still use CSI for stop detection. Fig. 5 (a) presents an example when it starts moving at about 400th sample. Observing the degree of disorder before and after the start, an intuitive method is to check for the deviation of amplitude, however, the sliding-window required by deviation checking reduces the checking sensitivity to movement. Fig. 5 (b) shows the slow raising deviation values with different length L_w of sliding window, and the detected time obviously lags behind.

The spatial de-correlation property of CSI gives us a hint. We find that the correlation coefficient ρ between consecutive CSI samples will drop rapidly if the spatial distance d_s between them is larger than $\lambda/2$. Thus, there will be a rapid co-efficiency raising or drop to check the "moving" and "static" status. Fig. 5 (c) shows the samples' correlation matrix. When device is static, stable and high correlation co-efficiency holds the entire upper-left area, while it disappears immediately when the device starts moving. Figure 5 (d) presents the moving averages of ρ with different sliding window length L_w, and the dropping of ρ is fast and clear. According to our experimental evaluation, a devices is said to be moving when ρ drops below 0.4, and the final detected time t_d is quite close to the actual time t_a.

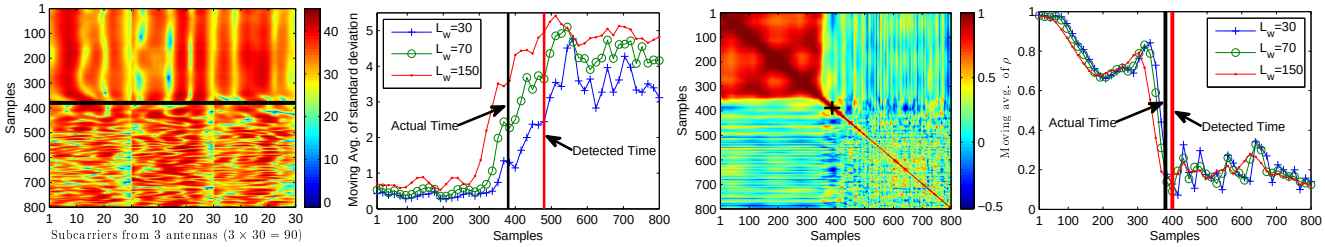

(a) (b) (c) (d)

Fig. 5. (a) the CSI image of a sample. The movement starts at about 400 time-slot. (b) the moving averages of standard deviation with different window lengths L_w. The detected start delays about 100 slot than actual start. (c) the correlation matrix of the CSI images shown in (a). (d) the moving averages of the correlation coefficients with different L_w.

4.4 Minimum Sampling Rate

Similar to sensor-based system, sufficient CSI sampling rate is critical for accuracy. Due to the un-equal time distribution between fading and non-fading, the Nyquist sampling rate of $f_s = 2 \cdot f_{max}$ is not sufficient. We carried out experiments to find the minimum f_s that can guarantee good accuracy. Evaluations are carried out in a wide range of channel frequencies including 2.4G (channel 1), 5.2Ghz (channel 40), 5.5G (channel 100) and the highest 5.8G(Channel 161). During the experiment, testers are walking at the same speed around $v = 1.3m/s$ and the mobile device in their hands are constantly transmitting beacon frames at 500hz. After the experiments, we simulate the sampling rate f_s from 20hz to 500hz by dropping frames uniformly. Fig. 6 presents the results. We can see from the figure that the estimated speed v continuously climbs when f_s is higher than Nyquist rate f_N, and the speed stops raising when f_s is about 4 times of $f_v = 2v/\lambda$. More experiments in other situations have also confirmed the $4 \cdot f_v$ sampling rate. Therefore if we set $f_{max} = 1.6m/s$, the minimum sampling rate is only 100 (or 250) frames/s in 2.4G (or 5.8G) environment, or equivalent to approximately 40KBps or 100KBps traffic.

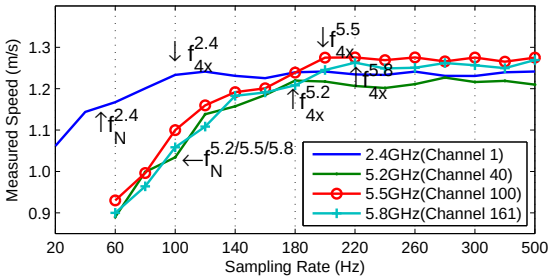

Fig. 6. The measured speeds in different sampling rate. The points denoted by $f_N^\star$ denotes the Nyquist sampling rate, while $f_{4x}^\star$ denotes the minimum require sampling rate.

The traffic burstiness is another problem. The burstiness, which happened frequently, is obviously against the CSI-based speed estimation. Since the burstiness is usually short-time high-frequency traffic phenomenon, a reasonable assumption could be made to ease this problem: people's walking speed remain stable during the gap between two burstiness. Fig. 7 presents our solution that during each burstiness the speed is estimated, while in the gap the speed is approximated as the average.

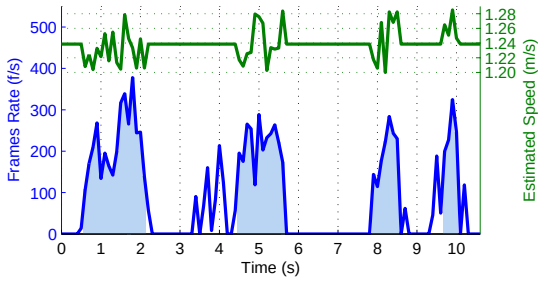

Fig. 7. The burstiness of wireless traffic in practical environment and the estimated speed.

5 RSS Fingerprints Extraction

RSS fingerprints are the most representative RSS points for given positions, and the error of the fingerprint will directly affect the accuracy. Besides the strong noise, we observed the directional shadowing problem which may easily break the traditional fingerprint extraction strategy.

5.1 The Directional Shadowing Problem

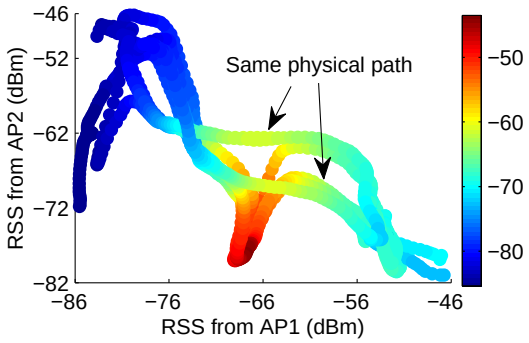

Fig. 8. RSS trajectories with 3APs. The color denotes the value for 3rd AP: deeper color denotes higher RSS from 3rd AP.

When people walk along the same path in different directions, the shadowing effect of human body will generate deviated RSS sample trajectories. Fig. 8 presents an example of such directional shadowing problem. Due to the strong directional shadowing, the same physical path corresponds to two parallel RSS trajectories. If applying clustering-based fingerprint extraction, the algorithm may wrongfully determine that there are two parallel paths between the start and end point. Thus, eliminating such directional shadowing is crucial for improving the localization accuracy.

5.2 Extracting Fingerprints

The RSS samples are highly deviated for the same physical position if under directional shadowing, however, the whole RSS changing trends are remarkably similar. Therefore extracting unique RSS fingerprints without directional shadowing could be transformed to a problem of correctly identifying the correspondence between a lot of RSS trajectories. Treating these trajectories as curve-shaped graphs, identifying the correspondence is, however, a n-partite graph matching problem. Fortunately, this can be done by $n-1$ times iteratively graph matching between n-th trajectory and previous resulting RSS fingerprints graph. As revisited in Section 2, relaxation-based approaches approximate the graph matching elegantly, and the only job is to build the affinity matrix $\mathcal{M}^{C^{P\times Q}}$ for two graphs G^P and G^Q.

A possible graph matching between G^P and G^Q is a set of assignments(or pairs) (i, i'), where $i \in V^P$ and $i' \in V^Q$. And for every two assignments $a = (i, i')$ and $b = (j, j')$, there is an *affinity score* $m_{a,b}$ that measures the compatibility between them. Let set $\mathcal{C}^{P\times Q}$ enumerates all possible assignments, then $\mathcal{M}^{P\times Q}$ is the affinity matrix of it, and $\mathcal{M}^{P\times Q}$ stores all the affinity scores for all possible assignments. Based on this definition, an optimal graph matching is a set of assignments C^* which has the highest inner affinity scores. Each element $m_{a,b} \in \mathcal{M}$ is assigned as follows in current

For visual clarity, we plot only RSS traces from 3 APs.

system.

$$\mathcal{M}_{(a,b)} = \begin{cases} e^{-||d_{ij}-d_{i'j'}||}, & \text{if } ||d_{ij}-d_{i'j'}|| > \epsilon \\ 0, & \text{otherwise} \end{cases} \tag{6}$$

where d_{ij} and $d_{i'j'}$ are the distance between i and j, and their assignment pairs i' and j', respectively. Since RSS attenuation along distance is non-linear, in our system the Minkowski distance [35] with value $p = 1.7$ is used to define the distance between RSS samples a and b.

$$d_{ab} = (\sum_{i=1}^{n} |rss_{ai} - rss_{bi}|^p)^{\frac{1}{p}} \tag{7}$$

where n represents the numbers of all heard APs, and rss_{ai} for the i-th AP's RSS value of RSS sample a.

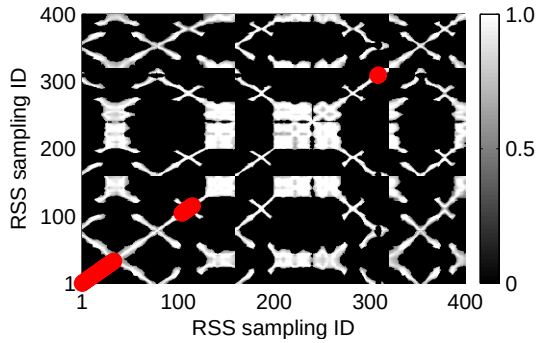

Fig. 9. The correspondence ratio among RSS sampling sequence. Ted dots denote the extracted RSS fingerprints.

After solving the graph matching problem with affinity matrix $\mathcal{M}$ using spectral approaches, the resulting column-wise vector $\mathcal{X}$ with length $n^P \times n^Q$ can then be reshaped to an *association matrix* $\boldsymbol{A}^{n^P \times n^Q}$, where each element $\boldsymbol{A}_{ij}$ denotes the *matching rate* between $i \in V^P$ and $j \in V^Q$. Due to the uniqueness, RSS fingerprints can be easily extracted by finding the RSS points which do not have correspondence in historical data. Let $\boldsymbol{U}_A$ be the upper triangular matrix of $\boldsymbol{A}$ and $\boldsymbol{D}_A$ for its diagonal matrix, a RSS point i is considered to be a RSS fingerprint **iff**

$$\sum_i (\boldsymbol{U}_A - \boldsymbol{D}_A) = 0.$$

Fig. 9 shows a sample association matrix for the graph matching between two same RSS trajectories. The red dots denote the extracted unique RSS samples points by graph matching algorithms, and they become effective fingerprints.

5.3 Fingerprints Transition Graph

The Fingerprints Transition Graph G^T records the spatial connections of all fingerprints. There are two conditions that qualify two nodes $i, j \in V(G^T)$ to have an edge $e_{ij} \in E^T$:

1. i and j are subsequent RSS fingerprints vector within the same RSS fingerprints segment;
2. i and j belong to different segments, the distance d_{ij} is smaller than ϵ and at least one of both is the *start* or *end* of a segment.

The weight of each edge e_{ij} is set to the geodesic distance between these two fingerprints measured by CSI speed estimation module.

6 Mapping Between Fingerprints and Floor Plan

6.1 Floor Plan in Manifold's Eyes

In human terms, the shortest distance between two points i and j in the indoor environment is not the euclidean distance $d_{eu}(i,j)$ but the geodesic distance $d_{geo}(i,j)$, which means that the indoor space in locally euclidean but globally not. In another words, indoor space could be essentially viewed as a 2D-manifold $\mathfrak{S}$ embedded in a 2D-polygon $\mathbf{P}$.

Since the geodesic distance reveals the true structure of the manifold, we resample the 2D floor plan with uniformly scattered points and construct an n-nodes graph G^M to represent the un-

folded version of the manifold. Any two nodes $i, j \in V^M$ have an edge e_{ij} **iff** the correspondence points i', j' in the floor plan $\mathbf{P}$ are in their mutual neighbourhood with *direct line-of-sight* distance, and the weight for edge is the direct distance that $e_{ij} = d_{eu}(i', j')$.

6.2 Unsupervised Accurate Mapping

Since the RSS samples are measured along users' walking trajectories, the RSS fingerprints transition graph G^T also share the same manifold structure. An intuitive solution to establish the fingerprint map is to apply graph matching directly between G^F and G^M. However, the accuracy and performance of large-scale graph matching (>50 points) is too poor for an unsupervised solution. A lightweight problem relaxation is to apply graphing matching only on corridor points graph. Once the corridor points graph are mapped correctly, the room matching is trivial. Unfortunately, the accuracy and performance of graph matching between such simple graphs is still not satisfied.

We devise a method called "Skeleton Matching" to achieve unsupervised accurate mapping between G^F and G^M even for very complex indoor structure. We first performs clustering on the corridor points to form a skeleton graph. Due to the high sparsity chain structure of G^F and G^M, the topology of the skeleton graphs follow exactly the structure of corridor points. As a highly condensed structure, performing graph matching on these graphs could achieve very high accuracy. Finally, once the skeleton graphs are correctly matched, the corridor points and the rooms will be matched trivially. The algorithm is detailed in following 3 steps, including skeleton graphs extraction, skeleton graphs matching, and find-grained points matching.

Extract the skeleton graph

Two sub-steps are required to extract the skeletons and the skeleton graphs. 1). Identifying the corridor points graph $G^{CF} \in G^F$ and $G^{CM} \in G^M$; 2). extracting skeleton graphs G^{SF} and G^{SM}.

In the first sub-step, a customized centrality measure $C(V)$ is designed to identify the core corridor network. For a given point $v \in V$, its centrality $C(v)$ is as follows.

$$C(v) = \sum_{s \neq v \neq t \in V} \sigma_{st}(v) \tag{8}$$

where $\sigma_{st}(v)$ is the numbers of shortest path from s to t via v.

Based on this definition, we design a iterative algorithm to remove the non-central points effectively. In each round of iteration, the centrality $C(v)$ is measured for every points. If $C(v)$ is smaller than a low-bound τ, then remove the points from the graph. This procedure repeats until no points is removed. The choose of value τ is critical. Too small τ will bring in redundant points, while overlarge τ will make all points be removed. Since the raise of τ will lead to monotonic decrease of number of remaining points, we use binary search method to find the critical τ^*.

In the second sub-step, the skeleton graphs V^S is generated by clustering the corridor points graph G^{CF} and G^{CM}. We use spectral clustering [36] (SC) as the clustering algorithm. SC is computationally faster than K-means and it only requires the similarity matrix which is exactly suitable in our case that both G^{CF} and G^{CM} are represented only in adjacency matrix. By clustering on G^{CF} and G^{CM}, we obtain the vertices set of skeleton graph G^{SF} and G^{SM}. The edge set E^{SF} and E^{SM} follow the underlying points, that if two points i, j, belonging to different clustersc_a and c_b respectively, have an edge, then there is an edge

between c_a and c_b. The weight of edge e_{ab} is defined as the shortest distance between the *central points* of cluster a and b, and the *central point* of a cluster is the point i which has the shortest distances to other points within the cluster.

Skeletons Matching

After the extraction of the skeleton graphs for both G^F and G^M, we then find the best correspondence between G^{SR} and G^{SM} via graph matching. Let symmetrical square matrix $\boldsymbol{M}^{SR}$ and $\boldsymbol{M}^{SM}$ represent their adjacency matrices. We build the affinity matrix $\boldsymbol{M}^{SR\times SM}$ for graph matching as follows.

$$\boldsymbol{M}^{SR\times SM} = e^{(\mathbf{1}^{SM}\bigotimes \boldsymbol{M}^{SR} - \mathbf{1}^{SR}\bigotimes \boldsymbol{M}^{SM})^2} \quad (9)$$

where $\bigotimes$ denotes the Kronecker product [37] and $\mathbf{1}^{SR}$ denotes the full-$\mathbf{1}$ matrix with the same size of G^{SR}.

We adopt RRWM algorithm [29] to perform the graph matching. Hungarian algorithm is further applied to discretize the $\mathcal{X}$ in order to meet the final integer constraints $\mathcal{X} \in \{0,1\}^n$.

Corridor Points Matching

Graph matching between G^{SF} and G^{SM} is quite easy. However, due to the inconsistency of clustering on G^{CF} G^{CM}, the matching between the skeletons graph cannot lead to the direct one to one points matching of two matched clusters.

In the corridor points graphs, only a few points connect multiple chain structures. Therefore, once we identify the correct correspondences of these *bridge points* V_b^{CF} and V_b^{CM}, the rest of the points can be matched subsequently. In order to identify the bridge node, we introduce a new metric called "bridge centrality", which is equal to the number of shortest paths from all vertices to all others within nearby clusters that pass through that node.

$$C_{bg}(v) = \sum_{\{(s,t)|v\in c^i, s,t\in NN(c^i), s,t\notin c^i\}} \sigma_{st}(v) \quad (10)$$

where $NN(c^i)$ denotes the nearby cluster of c^i. The bridge point will be the point with the highest bridge centrality.

After identifying the correspondence of bridge points in G^{CF} and G^{CM}, we next start the matching of the chain points in both graphes. Since the bridge points hold the main structure of the graphs, the enumeration of all the one-hop paths between any two bridge points will cover all the chains. For every one-hop path matched in both graphs, the points in G^{CF} are sequentially matched to G^{CF} according to distance information.

7 Localization and Tracking

C^{2}IL provides a unified localization and tracking service by treating the direction localization request as a tracking request without historical data. Here we mainly focus on tracking technique in **C^{2}IL**. Unlike the stateless K-NN based method which is widely adopted in previous approaches, in our solution, the users' trajectories are globally determined from the very beginning by transforming the tracking problem to a graph matching problem between the measured RSS samples transition graph G^S and the fingerprint transition graph G^T. After the graph matching, the accuracy is further improved by bringing in the CSI-based speed estimation through a particle-filter based fusion. Here we start introducing these two steps.

7.1 Graph Matching Based Tracking

Graph matching based tracking is to find the best correspondence between the sequence of RSS

samples of tracking request and extracted fingerprints. This is exactly the same matching process undertaken in Section 5, except for the differences that the tracking is to find the matched points, while in Section 5 the un-matched RSS samples are added to the fingerprints database.

Let $\mathcal{X}^{n^S \times n^F}$ represent the association matrix obtained through spectral matching where n^S and n^F are the numbers of RSS samples and candidate fingerprints respectively. Due to the error in RSS measurement and fingerprints map construction, a single RSS samples p_i may correspond to multiple fingerprints in $\mathcal{X}$,*e.g.*, a RSS sample may correspond to two fingerprints, one is in corridor, and another is in a room. Fortunately the temporal correlation can help eliminate those false correspondence by checking the spatial continuity between current and subsequent candidate fingerprints. After eliminating the false correspondence, the globally estimated coordinates sequence will be given by $T_{G^S} = f_{G^T}(G^S)$, where $f : fingerprint \rightarrow G^M$ represents the mapping from fingerprints to the floor plan manifold G^M, and T_{G^S} are the resulting coordinates sequence in G^M.

However, full graph matching between all fingerprints set and RSS samples is time-consuming, therefore a matching candidates pruning process is introduced to meet practical demand of real-time tracking of multiple clients.

Matching Candidates Pruning: The main idea of the pruning is to find the probable walking area for the tracking request using coarse-grained nearest neighbor (NN) method, which will significantly reduce the search space.

Let $R^T = \{r_1^T, .., r_n^T\}$ represent the RSS sequence of the tracking request at time t, where r_i is a n-dimensional RSS vector. The length n is smaller than a positive integer $\mathcal{L}$, such that the tracking algorithm provides limited backtracking. Let $R^F = \{r_1^F, .., r_n^F\}$ denote the RSS fingerprints set and graph G_P^F denote the positions of fingerprints in the floor plan. The pruned matching candidate set S_u is defined as follows.

$$S_u = \{r^F | r^F \in R^F, r^F \in \epsilon\text{-NN}_{\mathrm{R^F}}(\mathrm{NN}_{\mathrm{R^F}}(\mathrm{R^T}))\} \tag{11}$$

where $\mathrm{NN}_{\mathrm{R^F}}(\mathrm{R^T})$ denotes the nearest neighbors of R^T within the fingerprints set R^F, and ϵ-$\mathrm{NN_A(B)}$ denotes the B's neighborhood within distance ϵ in the set A. Here the ϵ is set to 3m.

7.2 Fine-Grained User Tracking

The movement estimation from trajectories matching (TM) and CSI-based speed estimation (CBSE) are naturally complementary. TM is slow-responsive yet accurate in long time, while CBSE may drift with time cumulation yet be accurate in short time. Obviously, a fusion scheme for TM and CBSE will significantly improve the accuracy. Due to the linearity constraints and difficulties in correctly estimating the error covariance matrices, we don't use the conventional Kalman filter. The more robust particle filter (PF) is adopted as the fusion algorithm.

The state space of the tracking is a two dimensional vector $\boldsymbol{X}_t = [M_i, vt]$, where M_i represents the i-th node in the floor plan manifold M, and v for the walking speed. The main challenge here is that the speed v has no direction information, therefore every round the PF evolves and there are multiple candidate predictions. For instance, when walking in a corridor without optional paths, there are two candidate directions, forward and backward, and therefore two state candidates $\boldsymbol{X}_{for} = [M_j, v_t]$ or $\boldsymbol{X}_{rev} = [M_h, v_t]$, where M_j and M_h are two nearby nodes in different directions.

Fortunately,the PF can handle this problem elegantly by sprinkling different amounts of parti-

cles in different directions. In the prediction phase of each filter iteration, the particles will be re-sampled and enumerate all possible candidate directions.

Fig. 10 illustrates the particles distribution along a path, in each round the particles enumerate all possible candidate directions. When there are optional paths, the particles will enumerate all possible options. After the fusion, the M_i is transformed to floor plan coordinates.

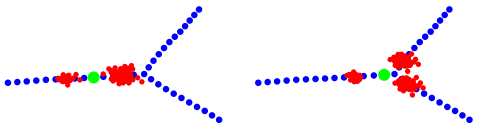

Fig. 10. The predicted particles distribution before each new measurement: red dots represent the particles, and green dots for the determined position in last round.

8 System Evaluation

8.1 Prototype System with Customized APs

We designed and developed a prototype hardware system for **C^{2}IL**. The prototype system is deployed in a large $2000m^2$ office environment with circular corridor network as shown in Fig. 11. To maximize the participation rate, **C^{2}IL** is deployed at AP-end. In total, 19 customized APs are sparsely deployed across the office that provide both wireless networking service and localization service. They will forward the measured RSS and CSI values to a central localization server. A developed simple client App is installed on testers' Android smartphones. The localization server will calculate the clients' position based on the networking traffic, and clients only need to read the location coordinate from server.

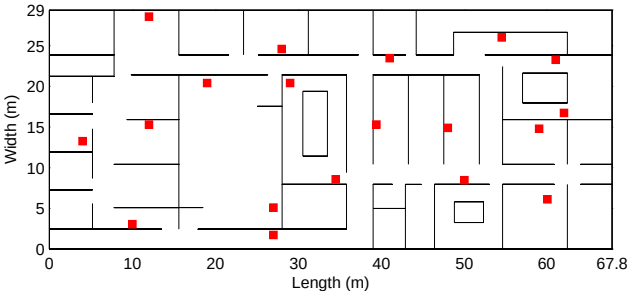

Fig. 11. The floor plan of our test area, and red dots denote the deployed customized APs.

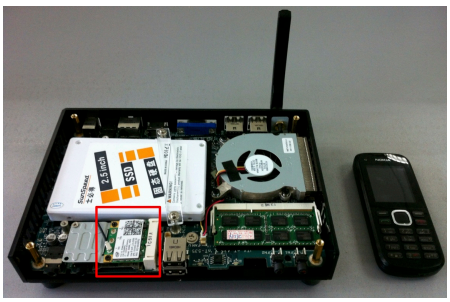

Fig. 12. Prototype system for **C^{2}IL** with Intel Atom-based Mini PC and 5300NIC as AP.

Although CSI is a standard PHY layer information, currently only Intel 5300 NIC can export it to user level. Our customized AP is simply an Intel ATOM- based mini PC with 5300 NIC. Figure 12 shows our customized AP. It equips with single-core 1.6Ghz ATOM CPU and 5300 NIC. The total cost is about $90. The OS is Ubuntu 12.04 64-bit, and AP function is hosted by hostapd. Besides the ordinary AP interface, a monitor virtual interface is also added to overhear the wireless traffic. Both measured CSI and RSS are uploaded to localization server in real-time.

8.2 C^{2}IL Speed and Distance Estimation

In this experiment, 10 students are asked to walk 3 times around the $129m$ long circular corridor as shown in Fig. 11. They are asked to maintain constant walking speed in first round, and the speed may change slightly and remarkably in second and third round. The measured speed will

be integrated to walking distance D_w. We mainly considered the error rate $e_w = |D_{path} - D_w|/D_{path}$.

Two other speed estimation approaches *i.e.* pedometer-based and channel coherent-time based [28], are also developed as comparison. For pedometer we use NASC [2] method to detect steps, and the step length is predefined in training phase. The accelerometer data required by the algorithm was retrieved from laptop's HD active protection. For coherent-time based approaches, we use a constant $\xi = 0.396$, which is manually optimized for this evaluation.

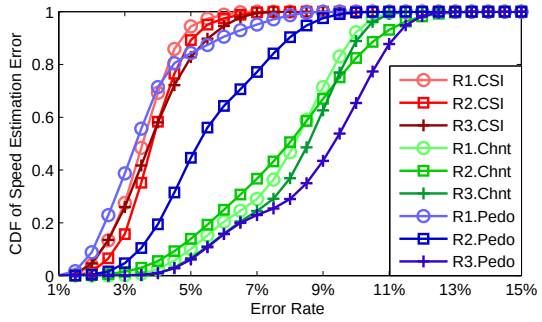

Fig. 13. The Error CDF of 3 methods.

Fig. 13 presents the error CDF of three methods in three walking manners: with constant speed (R1), slightly varying speed (R2), and with marked change (R3). The experiment shows that, comparing to pedometer- based approach, **C^{2}IL** with CSI can achieve better accuracy without requiring predefined constants or training data, meanwhile, **C^{2}IL** significantly outperforms pedometer-based (Pedo) approaches when speed is varying or pre-defined step length is out of effectiveness. Coherent-time based approach (Chnt) haves the similar speed-invariance feature, however, the accuracy is considerably poorer than **C^{2}IL** and pedometer in constant speed.

The accuracy of CSI-based distance estimation is then evaluated. To evaluate the influence of richness of multipath components to the distance estimation error, we carried out experiments in 3 typical environments, a compact corridor, a large office environment, and a very large hall. In each environment we walked along a 50m straight line for 10 times. Two APs were simultaneously used to estimate walking distance. One was placed at the end of the path with strong LoS component, and the other was placed in a cubicle to cut-off the LoS components to simulate strong Rayleigh fading. Figure 14 (a) plots the Rician K Factor [38] along the walking path in different environment, which estimate the degree of LoS components. Very low and stable K appears in corridor environment which means there are rich multipath components, while in office and hall the multipath components is significantly reduced due to the weak reflection in large wide-open space. Figure 14 (b) and (c) plot the CDF of estimated walking distance by the AP in path and cubicle respectively. We see in the best situation that in a corridor with strong multipath component, there is only 3% error. In Figure 14 (c), we also see small error happened in the path, and in the worst situation, in a large hall with very weak multipath components, the averaged estimated error is less than 10%.

8.3 Mapping Accuracy Test

Fig. 15 (a) shows extracted corridor points and the "bridge points". The critical τ^* is set to 127 after 6 round of iteration. To obtain the RSS transition graph, 5 students are asked to walking in the rooms for 20 minutes to cover all accessible area. The RSS and CSI data is collected, and Fig. 15 (b) and (b) shows the visualization of G^T and G^{CT} respectively. Please note that our mapping algorithm requires only the adjacency matrix of graphs, and the MDS-based position is only for visualization. The graph matching result is shown in figure (d). For each graph G^{SF} or G^{SM} there are 8 points, the graph matching under such small scale could achieve stably and accurate

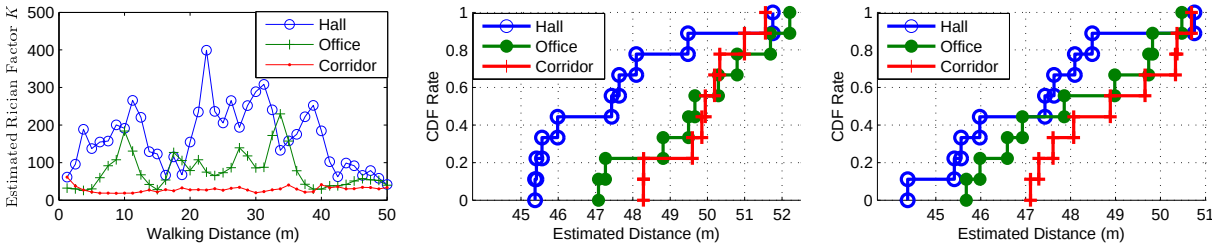

(a) Racian Factor K (b)Strong Rayleigh Fading (c) Weak Rayleigh Fading

Fig. 14. (a) the Rician factor K along the path in different environment. (b) the CDF of estimated distance without LoS components (c) the CDF with strong LoS components.

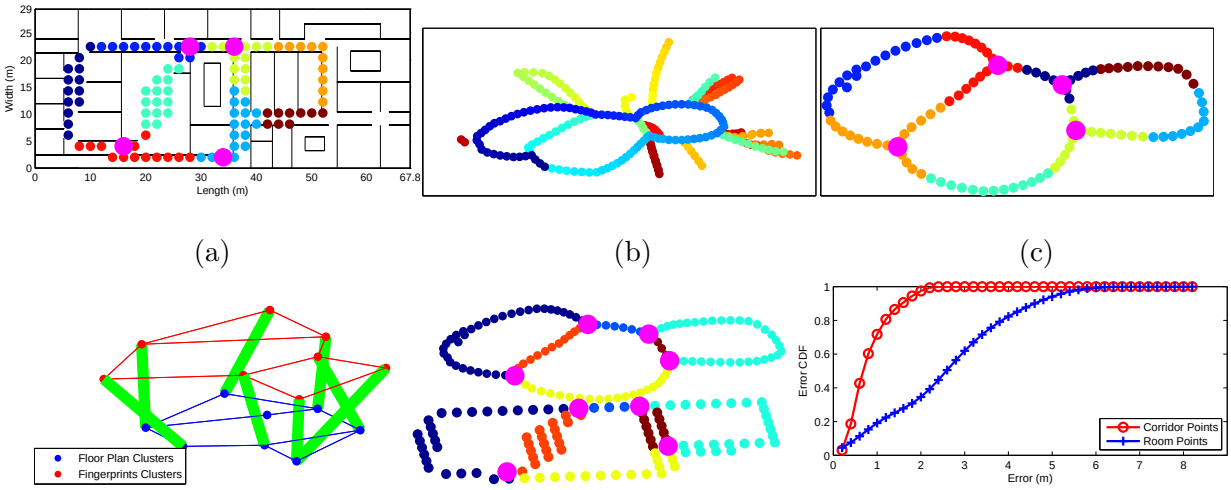

(a) (b) (c)

(d) (e) (f)

Fig. 15. (a) The clustering of corridor points graph G^{CM}, the purple points denotes the "bridge points". (b) An visualization of RSS fingerprints transition graph G^T. (c) The clustering of the G^{CT} (the corridor points of G^T). (d) The skeleton matching result between G^{ST} and G^{SM}. (e) The matching between G^{CT} and G^{CM} under the guide of skeleton matching and the "bridge points", the same color denotes the correspondence. (f) The room matching accuracy CDF.

mapping. Figure (e) shows the matching of corridor points under the guide of skeleton matching and the "bridge points". Figure (f) shows the error of both corridor points mapping and room points mapping. We can see clear that the corridor points are highly matched. The corridor points maximum error is still under 2m, while the maxmium room matching error is under 6m.

8.4 Localization and Tracking

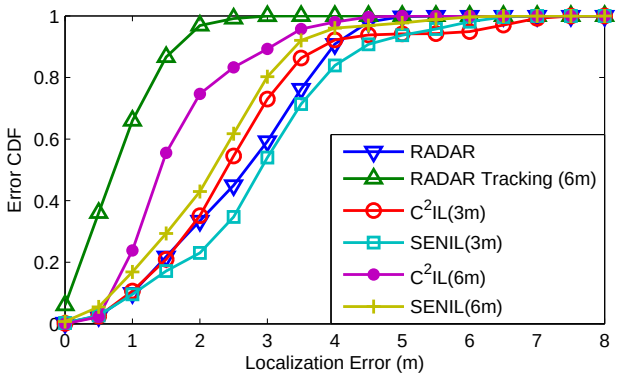

Fig. 16. The localization & tracking error CDF with different amount of historical RSS fingerprints data. The RADAR scheme is as comparison. The suffix number (0m) denotes the direct single point localization, while (10m) denotes the tracking service with a historical data of 10m.

In this test, we compared **C^{2}IL** with our previous work **SENIL** [16], and RADAR [10] system still worked as baseline. the RSS/CSI samples of 20 minutes walking in different speeds are used as testing data. Since we mainly evaluated the accuracy with different length of historical data, we randomly select ℓ successive RSS samples for each round. Figure 16 plots the error CDF with different amount of historical data. Comparing to SENIL, **C^{2}IL** is averagely 1m better. The accuracy improvement is mainly due to the precise moving speed/distance estimation.

9 Conclusion

In this paper, we proposed an indoor localization and tracking scheme, **C^{2}IL**. Our scheme does not require using additional sensors, except the availability of 802.11n wireless connection. We believe that **C^{2}IL** is the first scheme that the really benefits from the multipath effect in complex environment. An innovative method is proposed to accurately estimate the moving speed and distance purely based on 802.11n CSI, which should find a wide range of applications alone. Based on this accurate distance estimation, we built the mapping between RSS fingerprints and location using unsupervised learning, and unified the localization and tracking. Our extensive evaluation results indicate that our scheme **C^{2}IL** successfully handles very complex indoor structure and simultaneously provides the best performance in contribution rate, localization cost, and localization/tracking accuracy.

References

[1] Sen S, Choudhury R R, Nelakuditi S. Spinloc: Spin once to know your location. Proceedings of the Twelfth Workshop on Mobile Computing Systems & Applications, 2012, p.12.

[2] Rai A, Chintalapudi K K, Padmanabhan V N, Sen R. Zee: zero-effort crowdsourcing for indoor localization. Proceedings of the 18th annual international conference on Mobile computing and networking, 2012, pp.293–304.

[3] Nandakumar R, Chintalapudi K K, Padmanabhan V N. Centaur: locating devices in an office environment. Proceedings of the 18th annual international conference on Mobile computing and networking, 2012, pp.281–292.

[4] Liu H, Gan Y, Yang J, Sidhom S, Wang Y, Chen Y, Ye F. Push the limit of wifi based localization for smartphones. Proceedings of the 18th annual international conference on Mobile computing and networking, 2012, pp.305–316.

[5] Yang Z, Wu C, Liu Y. Locating in fingerprint space: wireless indoor localization with little human intervention. Proceedings of the 18th annual international conference on Mobile computing and networking, 2012, pp.269–280.

[6] Rappaport T S, et al. Wireless communications: principles and practice. Prentice Hall PTR New Jersey, 1996.

[7] Liu J, Priyantha B, Hart T, Ramos H S, Loureiro A A, Wang Q. Energy efficient gps sensing with cloud offloading. Proceedings of the 10th ACM Conference on Embedded Network Sensor Systems, 2012, pp.85–98.

[8] Zhao J, Xi W, He Y, Liu Y, Li X Y, Mo L, Yang Z. Localization of wireless sensor networks in the wild: pursuit of ranging quality. *IEEE/ACM Transactions on Networking (TON)*, 2013, 21(1):311–323.

[9] Bo C, Ren D, Tang S, Li X Y, Mao X, Huang Q, Mo L, Jiang Z, Sun Y, Liu Y. Locating sen-

sors in the forest: A case study in greenorbs. INFOCOM, 2012 Proceedings IEEE, 2012, pp.1026–1034.

[10] Bahl P, Padmanabhan V N. Radar: An in-building rf-based user location and tracking system. INFOCOM, 2012 Proceedings IEEE, 2000, pp.775–784.

[11] Youssef M, Agrawala A. The horus location determination system. *Wireless Networks*, 2008, 14(3):357–374.

[12] Azizyan M, Constandache I, Roy Choudhury R. Surroundsense: mobile phone localization via ambience fingerprinting. Proceedings of the 15th annual international conference on Mobile computing and networking, 2009, pp.261–272.

[13] Sen S, Radunovic B, Choudhury R R, Minka T. You are facing the mona lisa: spot localization using phy layer information. Proceedings of the 10th international conference on Mobile systems, applications, and services, 2012, pp.183–196.

[14] Constandache I, Choudhury R R, Rhee I. Towards mobile phone localization without war-driving. INFOCOM, 2010 Proceedings IEEE, 2010, pp.1–9.

[15] Guha S, Plarre K, Lissner D, Mitra S, Krishna B, Dutta P, Kumar S. Autowitness: locating and tracking stolen property while tolerating gps and radio outages. *ACM Transactions on Sensor Networks (TOSN)*, 2012, 8(4):31.

[16] Jiang Z, Zhao J, Han J, Tang S, Zhao J, Xi W. Wi-fi fingerprint based indoor localization without indoor space measurement. Mobile Ad-Hoc and Sensor Systems (MASS), 2013 IEEE 10th International Conference on, 2013, pp.384–392.

[17] Halperin D, Hu W, Sheth A, Wetherall D. Tool release: gathering 802.11 n traces with channel state information. *ACM SIGCOMM Computer Communication Review*, 2011, 41(1):53–53.

[18] Yang Z, Zhou Z, Liu Y. From rssi to csi: Indoor localization via channel response. *ACM Computing Surveys (CSUR)*, 2013, 46(2):25.

[19] Jiang Z, Zhao J, Li X Y, Han J, Xi W. Rejecting the attack: Source authentication for wi-fi management frames using csi information. INFOCOM, 2013 Proceedings IEEE, 2013, pp.2544–2552.

[20] Xi W, Zhao J, Li X Y, Zhao K, Tang S, Liu X, Jiang Z. Electronic frog eye: Counting crowd using wifi. 2014.

[21] Han J, Qian C, Ma D, Wang X, Zhao J, Zhang P, Xi W, Jiang Z. Twins: Device-free object tracking using passive tags. 2014.

[22] Xiong J, Jamieson K. Arraytrack: a fine-grained indoor location system. Usenix NSDI, 2013.

[23] Adib F, Katabi D. See through walls with wifi! Proceedings of the ACM SIGCOMM 2013 conference on SIGCOMM, 2013, pp.75–86.

[24] Wang J, Katabi D. Dude, where's my card?: Rfid positioning that works with multipath and non-line of sight. Proceedings of the ACM SIGCOMM 2013 conference on SIGCOMM, 2013, pp.51–62.

[25] Adib F, Kabelac Z, Katabi D, Miller R C. 3d tracking via body radio reflections. 2014.

[26] Azemi G, Senadji B, Boashash B. Mobile unit velocity estimation based on the instanta-

neous frequency of the received signal. *Vehicular Technology, IEEE Transactions on*, 2004, 53(3):716–724.

[27] Mohanty S. Vepsd: a novel velocity estimation algorithm for next-generation wireless systems. *Wireless Communications, IEEE Transactions on*, 2005, 4(6):2655–2660.

[28] Pricope B, Haas H. Experimental validation of a new pedestrian speed estimator for ofdm systems in indoor environments. Global Telecommunications Conference (GLOBECOM 2011), 2011 IEEE, 2011, pp.1–5.

[29] Cho M, Lee J, Lee K M. Reweighted random walks for graph matching. In *Computer Vision–ECCV 2010*, Springer, 2010, pp.492–505.

[30] Leordeanu M, Hebert M. A spectral technique for correspondence problems using pairwise constraints. Computer Vision, 2005. ICCV 2005. Tenth IEEE International Conference on, 2005, pp.1482–1489.

[31] Sklar B. Rayleigh fading channels in mobile digital communication systems. i. characterization. *Communications Magazine, IEEE*, 1997, 35(7):90–100.

[32] Sheriff I, Belding-Royer E. Multipath selection in multi-radio mesh networks. Broadband Communications, Networks and Systems, 2006. BROADNETS 2006. 3rd International Conference on, 2006, pp.1–11.

[33] Yang S C. OFDMA system analysis and design. Artech House, 2010.

[34] Hill D A. Electromagnetic fields in cavities: deterministic and statistical theories. John Wiley & Sons, 2009.

[35] Groenen P J, Jajuga K. Fuzzy clustering with squared minkowski distances. *Fuzzy Sets and Systems*, 2001, 120(2):227–237.

[36] Von Luxburg U. A tutorial on spectral clustering. *Statistics and computing*, 2007, 17(4):395–416.

[37] Weichsel P M. The kronecker product of graphs. *Proceedings of the American Mathematical Society*, 1962, 13(1):47–52.

[38] Doukas A, Kalivas G. Rician k factor estimation for wireless communication systems. Wireless and Mobile Communications, 2006. ICWMC'06. International Conference on, 2006, pp.69–69.

Dr. Jizhong Zhao He is a Professor at the Department of Computer Science and Technology, Xi'an Jiaotong University. His research interests include computer software, pervasive computing, distributed systems, network security. He is a member of CCF, ACM, and IEEE.

Zhiping Jiang is a Ph.D candidate at Xi'an Jiaotong University, Xi'an. His research interests include localization, smart sensing, wireless communication, and image processing. He is a student member of IEEE.

Dr. Xiang-Yang Li is a professor at the Illinois Institute of Technology. He holds EMC -Endowed Visiting Chair

Professorship at Tsinghua University. He currently is distinguished visiting professor at Xi' An JiaoTong University, University of Science and Technology of China, and TongJi University. His research interests include mobile computing, cyber physical systems, wireless networks, security and privacy, and algorithms. He is a senior member of IEEE and a member of ACM.

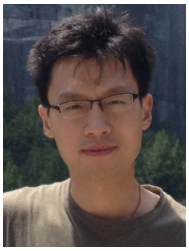

Dr. Shaojie Tang is an assistant professor at the University of Texas at Dallas. He received his Ph.D degree from Illinois Institute of Technology. His research interests include smart grid, sensor network, algorithm, and wireless security.

Dr. Jinsong Han is currently an associate professor at Xi'an Jiaotong University. He received his Ph.D. degree from Hong Kong University of Science and Technology. His research interests include pervasive computing, distributed system, and wireless network. He is a member of IEEE and ACM.

Dr. Wei Xi is a postdoctoral research fellow at Xi'an Jiaotong University. His main research interests include wireless networks, smart sensing, and mobile computing. He is a member of CCF, ACM, and IEEE.

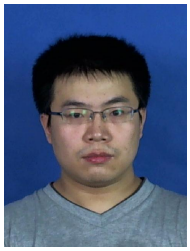

Kun Zhao is an Ph.D candidate at Xi'an Jiaotong University, Xi'an. His research interests include signal processing, wireless communication, smart sensing, and algorithm.

Zhi Wang is an Ph.D candidate at Xi'an Jiaotong University, Xi'an. His research interests include smart sensing, pervasive computing, localization, and wireless security.